BNL-112237-2016-JA

Transition metal nitride coated with atomic layers of Pt as low-cost and high-stable electrocatalysts for oxygen reduction reac

X. Tian

Submitted to Journal of the American Chemical Society

February 2016

Chemistry Department

Brookhaven National Laboratory

U.S. Department of Energy
[DOE Office of Science]

DISCLAIMER

Transition metal nitride coated with atomic layers of Pt as low-cost and high-stable electrocatalysts for oxygen reduction reaction

Xinlong Tian[1], Junming Luo[1], Haobing Zou[1], Rong Chen[1], Ting Shu[1], Xiuhua Li, Yingwei Li[1], Huiyu Song, Shijun Liao[1,], Dong Su[2], Radoslav R. Adzic[2,]**

1. The Key Laboratory of Fuel Cell Technology of Guangdong Province & the Key Laboratory of New Energy Technology of Guangdong Universities, School of Chemistry and Chemical Engineering, South China University of Technology, Guangzhou 510641, China

2. Chemistry Department, Brookhaven National Laboratory, Upton, NY 11973, USA

Abstract

The high cost caused mainly by the usage of precious Pt to against sluggish kinetics of the oxygen reduction reaction (ORR) at the cathode, catalyst degradation and carbon-support corrosion are three of the most challenges for the commercial viability of polymer electrolyte membrane fuel cells (PEMFCs). To address these obstacles, we aimed towards carbon-free and robust transition metal nitride (TMN) with low Pt content materials exhibited tunable physical and catalytic properties. Here, we report a high performance low Pt catalyst prepared by covering Pt atoms on the nanoparticles of titanium nickel binary nitride (TiNiN) with several atomic layers. Towards the oxygen reduction reaction (ORR), the novel catalyst exhibited over 400% increase in mass activity and over 200% increase in specific activity when compared with the commercial Pt/C catalyst. The catalyst also showed excellent stability/durability, after 10, 000 potential cycles, only a slight performance loss could be observed, meanwhile, the structure of the catalyst was perfectly maintained, as established by TEM results. The outstanding performance of the catalyst may be resulted from the ultra high dispersion of Pt (several atoms layer coated on the nitride nanoparticles), and the excellent stability/durability may arise from the good stability of nitride, and the synergetic effects between ultra thin Pt layer and the robust TMN support. Actually, no Pt diffraction can be detected by XRD analysis and no Pt nanoparticles can be observed by TEM measurements for Pt coated nitrides, but Pt can be detected

by the XPS, and its thin layer can be observed by the HRTEM on the surface of nitride nanopartilces, confirming the high dispersion of Pt on the surface of nitride nanoparticles. Further, the significant shift of Pt 3d binding energy evidences the interaction between Pt and nitrides.

Keywords: transition metal nitride, ultra thin Pt layer, oxygen reduction reaction, catalyst stability, fuel cells

1. Introduction

Low-temperature polymer electrolyte membrane fuel cells (PEMFCs) are attracting great attention as a promising power source for transportation and residential applications due to their pollutant-free operation and high energy conversion efficiency [1-4]. However, the development of PEMFCs is severely hampered by the fact that the sluggish of oxygen reduction reaction (ORR) and the use of platinum (Pt) as the electrocatalyst, which is expensive and scarce [5-8]. The design and fabrication of highly active and stable ORR catalysts with low cost is extremely desirable but remains challenging. A number of methods have been proposed for exploring new electrocatalysts with low Pt loadings, including alloying Pt with secondary transition metals [9-11], depositing atomic layers of Pt onto other fine metal particles to create core/shell structure [12-15] and dealloying approach [16, 17]. Specially, the core/shell structure with Pt present around the thin shell of the core not only minimizes the Pt use and maximizes the Pt exposure to oxygen, but also introduces the expected core–shell interactions to tune both electronic and surface strain effects for optimal catalysis [12, 18]. Although the studies have led great improvements to catalyst performance, the core elements used in these works are still costly metals, such as Pd [13, 19-21], Au [22], Ir [23-25] and Ru [26, 27]. In addition, the carbon black is still the most widely used electrocatalyst support for ORR, corrosion of carbon support by electrochemical oxidation in fuel cell operating conditions, resulting in precious metals aggregation and separation from the carbon support, then causing a degradation in performance have been extensively reported [28-33]. These catalysts exhibit high precious metal content and also lack durability as harsh oxidation conditions lead to their loss of electrochemical surface area (ECSA)

and the fuel cell performance, encumbering the development of highly active, stable and low cost cathode electrocatalysts.

Recently, transition metal nitrides (TMNs) supports are regarded as ideal candidates for noble metal catalyst supports in PEMFCs because they are highly electrically conductive (metallic), thermally stable with exceptional hardness (covalent), and corrosion resistance in fuel cell operating conditions [2, 34-37]. They are also able to affect the electrocatalytic activity of the supported noble metals due to metal−support interactions. TMN materials supported Pt (Pt/TMNs) catalysts with better ORR performance and durability than commercial Pt/C catalysts have been reported [38-41]. It is believed that the Pt/TMN catalyst exhibit strong metal-support interaction (SMSI) that therefore the Pt nanoparticles (NPs) adhere to the support more strongly than that of the carbon support, facilitating their stabilization and electron transference during the catalysis process. However, the catalytic potential, Pt utilization and the low cost of the supported Pt NPs may not be fully realized. To this end, one would expect assemble a core/shell-like structured Pt@TMN catalyst that based on the promising data obtained from both core/shell and Pt/TMNs catalysts.

Herein, we report a Pt@TiNiN catalyst, which was prepared firstly by nitrating the ammonia complex of Ti and Ni at 700^{o}C in NH_3 atmosphere, following by depositing a Pt shell on the TiNiN nanoparticles with a pulse deposition approach, the Pt coated on the nitride nanoparticles with a thickness of several Pt atoms but not nanoparticles. Such an approach would solve both the problem of poor utilization and degradation of the catalyst related to carbon-support corrosion as well as the combination of high catalytic activity with sufficient low Pt loading. Amazingly, the catalyst exhibits surprisingly high activity and superior stability for the oxygen reduction reaction (ORR) in acid solutions. The mass activity of the our catalyst is up to 0.83 Amg^{-1}_{Pt} at 0.9 V, which is four-fold as respect to that of the commercial carbon-supported Pt catalyst (20wt% Pt on Vulcan XC-72, JM Pt/C).

2. Experimental Procedures

2.1 Synthesis of TMN NPs

TMN NPs was prepared by a complexation-nitridation approach. Take the preparation of $Ti_{0.95}Ni_{0.05}N$ (labeled as TiNiN) as example, firstly, titanium tetrachloride ($TiCl_4$, 1 mL) and nickel acetate tetrahydrate ($Ni(CH_3COO)_2{\cdot}4H_2O$, 0.119 g) were dissolved in 30 mL of ethanol under stirring. , then the NH_3 gas was introduced to the solution (40 sccm min^{-1}) with continuous stirring for 30 min, the precipitate of complex was formed. After that, the mixture was transferred to a vacuum drying oven and kept at 80°C overnight to evaporating ethanol solvent. Secondly, the complex powder was placed in the tubular furnace, and nitrided at 700°C under the NH_3 gas flow (100 sccm min^{-1}) for 2 h, then the sample was cooled to room temperature under the protection of argon flow. For comparison, TiN NPs were synthesized with the same processes as $Ti_{0.95}Ni_{0.05}N$ but without the addition of $Ni(CH_3COO)_2{\cdot}4H_2O$ in the precursors.

2.2 Preparation of Pt@TMN catalyst

Pt extra-thin layer was deposited on the TMN NPs with a pulse electro-deposition (PED) process developed by our group [22, 24]. 5 mg of this TMNs was put into 1 mL Nafion/ethanol (0.25 wt% Nafion) solution through ultrasonic dispersion to form a slurry, and 4 μl of this slurry was pipetted onto a glassy carbon (5mm inner diameter, 0.196 cm^{-2}) surface to function as a substrate. A compostion of $H_2PtCl_6{\cdot}6H_2O$ (5 mmol), polyvinylpyrrolidone (PVP, 50 mmol) and 0.5 M H_2SO_4 solution was used as the electrolyte, and a PED procedure was applied to deposit Pt layer on the surface of the TMN NPs, the T_{on} (the time of connection) and T_{off} (the time of disconnection) used in this work are 0.003 s and 0.03 s, respectively. The theoretical deposited amount of Pt is calculated from the total deposition charge, and the actual Pt loading is determined by inductively coupled plasma optical emission spectrometry (ICP-OES, Leeman PROFILE SPEC) measurements analysis. It was found that the actual deposited amount is about one sixth of the theoretical deposited amount, and the deposited amount used in this paper is the actual amount analyzed by ICP-OES. Because no Pt nanoparticles could be observed/detected by XRD and TEM, we denoted the

catalysts prepared in this work as Pt@TiNiN and Pt@TiN when TiNiN and TiN were used as the substrates, respectively, although they may not have perfect/complete core-shell structure.

2.3 Physical characterization of the catalysts

X-ray diffraction (XRD) was conducted on a TD-3500 powder diffractometer (Tongda, China) operated at 30 kV and 20 mA, using Cu-K radiation sources in the Bragg angle ranging from 20° to 86°. Energy dispersive X-ray analysis (EDX) was performed with a field-emission scanning electron microscope (FE-SEM, Hitachi S-4800). Transmission electron microscopy (TEM) and high-resolution Transmission electron microscopy (HR-TEM) images were acquired with a JEOL 2100 microscope. X-ray photoelectron spectroscopy (XPS) was performed on an Axis Ultra DLD X-ray photoelectron spectrometer employing a monochromated Al-Ka X-ray source (hv=51486.6 eV). The Brunauer-Emmett-Teller (BET) surface area and pore distribution were measured by nitrogen adsorption-desorption on a Tristar II 3020 gas adsorption analyzer.

2.4 Measurements of the electrocatalytic performance of the catalysts

All the electrochemical measurements were carried out on an electrochemical workstation (Ivium, Netherlands) at room temperature (25±1°C), using a three-electrode electrochemical setup with a rotating disk electrode (RDE) system (Pine Research Instrumentation, USA). The cell consisted of a glassy carbon working electrode (GCE, 5 mm inner diameter, 0.196 cm^2), a platinum wire counter electrode and an Ag/AgCl (saturated 3M NaCl) reference electrode. All potentials in this work are quoted with respect to the reversible hydrogen electrode (RHE).

The catalyst electrode was prepared as follows: first, a catalyst ink was prepared by ultrasonicating the mixture of 5.0 mg catalyst and 2 mL Nafion (0.25 wt.%) ethanol solution for 30 min. Subsequently, 8 mL catalyst ink was piped onto the GCE surface. Finally, the GCE was dried under an infrared lamp for 5 min. The Pt loading was calculated from the content of Pt in Pt@TMN catalyst. For JM Pt/C catalyst (3.3 nm, 20

wt% Pt supported on Vulcan XC-72 R carbon), the Pt loading on the RDE is 5.61 μgcm^{-2}.

Cyclic Voltammetry (CV) characterization of the catalysts in the absence of oxygen was typically carried out in the potential range from 0.1 to 1.3 V at a scan rate of 50 mVs^{-1} in N_2-saturated 0.1 M $HClO_4$ solution. The ORR polarization curves were recorded in O_2-saturated 0.1 M $HClO_4$ electrolyte at a rotation rate of 1600 rpm at a scan rate of 10 mVs^{-1}. The accelerated durability test (ADT) for the catalysts was performed in O_2-saturated 0.5 M H_2SO_4 solution in the potential range from 0.6 to 1.05 V at room temperature.

3. Results and discussions

Figure 1 shows the powder XRD patterns of as-prepared TiN and TiNiN NPs, respectively. The TiN and TiNiN NPs exhibit characteristic peaks of the face centered cubic (fcc) TiN phase (JCPDS No. 38-1420). After the high temperature nitridation process, only the TiN phase (fcc) could be detected, suggesting that all the complex precursors were successfully converted to TiN nanostructures. For TiNiN NPs, the locations of diffraction peaks are almost identical to those of TiN NPs, indicating that the Ni atoms entered the lattice of TiN with a substitution of Ti atoms. However, obvious peak shift could be observed in the XRD patterns of TiNiN, the compression of the unit cell parameters may be caused by the smaller atom radius of Ni (0.056 nm) than that of the Ti atom (0.067 nm). It is noted that no signals corresponding to Ni metal, Ni oxides or phase separation between Ti and Ni nitride, suggesting that that the effective incorporation of Ni into the TiN (fcc) structure to form a single-phase solid solution. The composition profile of TiNiN demonstrated a Ti:Ni atomic ratio of 46.91:2.50, which agrees well with the expected atomic ratio of 19:1 that used in the precursors. This confirmed that our method is facile and the composition of the binary TMNs can be controlled without the help of any template or surfactant.

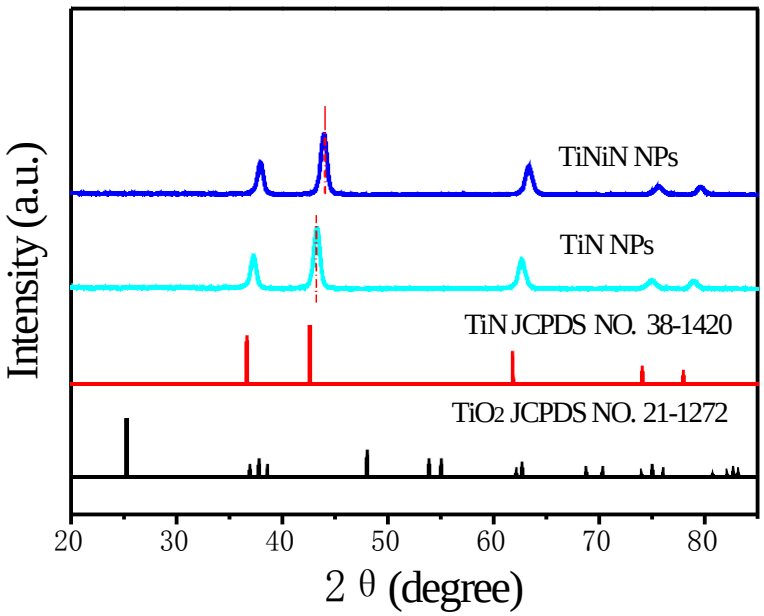

Figure 1. XRD patterns of as-prepared TiN and TiNiN NPs

Typical transmission electron microscopy (TEM) images were used to observe the morphology of TiN and TiNiN NPs. Aggregation of TiN and TiNiN NPs could be observed in the TEM images, as shown in Figure 2, TiN NPs exhibited spherical nanostructure, however, for TiNiN material, some cubic morphologies could be observed clearly (Figure 2d). According to the results of XRD, the crystallite sizes of TiN and TiNiN are ca. 9.8 nm and 9.2 nm, respectively, much smaller than those previously reported free-standing TMN NPs [42, 43]. Figure S1 presented the selected area electron diffraction (SAED) pattern of TiN NPs, some concentric rings, composed of bright discrete diffraction spots, could be observed, which were indexed to (331), (400), (222), (311), (220), (200), and (111) crystal planes of TiN (fcc) structure, demonstrating the high degree of crystalline of individual TiN NPs.

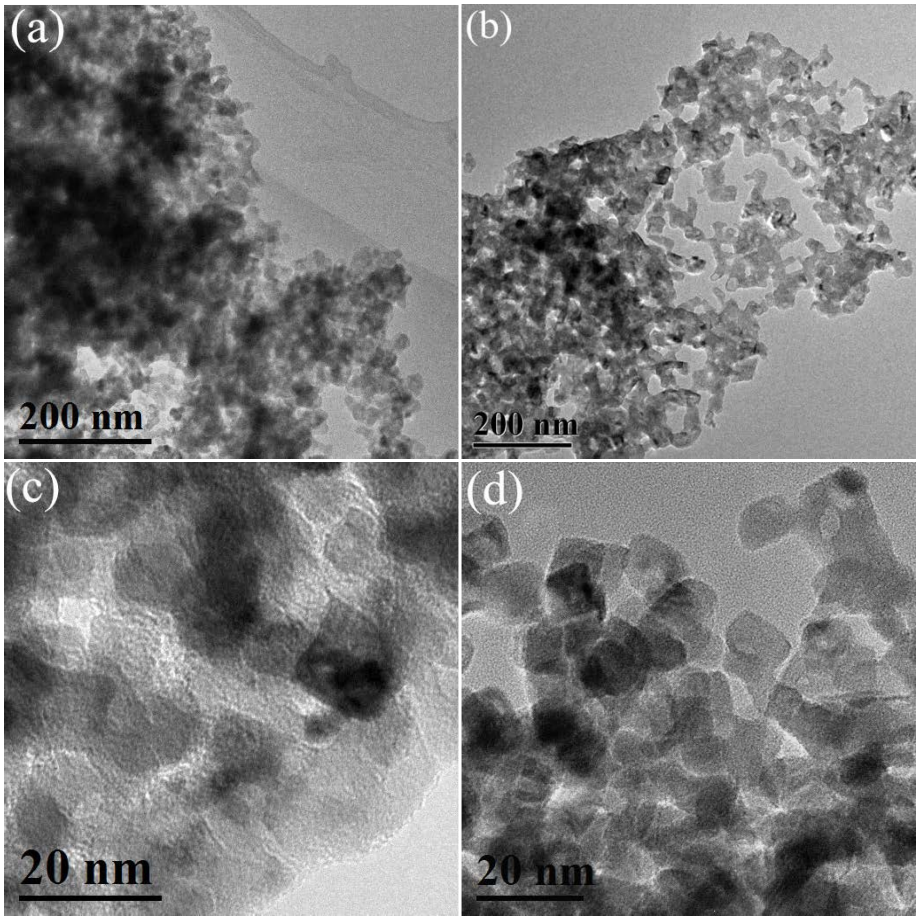

Fig. 2. TEM images of (a,c) TiN and (b,d) TiNiN NPs, respectively..

The detailed structural feature of TiN and TiNiN NPs were characterized by high-resolution TEM (HR-TEM), as shown in Figure S2. The well-defined crystalline lattice can be observed with a lattice spacing of 0.251 and 0.250 nm for TiN and TiNiN, respectively, corresponding to the (111) plane of TiN (fcc) [44], which are consistent with the XRD results.

Figure 3 shows the TEM and HRTEM images of Pt@TiNiN and the images of Pt@TiN are presented in Figure S3. As can be seen, no any Pt NPs could be found from both of the two samples. However, some lattice fringes, which is corresponding well to the interplane spacing of Pt (111) planes (0.227 nm) [45, 46] could be observed clearly, suggesting that the Pt may existed on the surface of the nitrides as extra-thin layer (several atoms thickness).

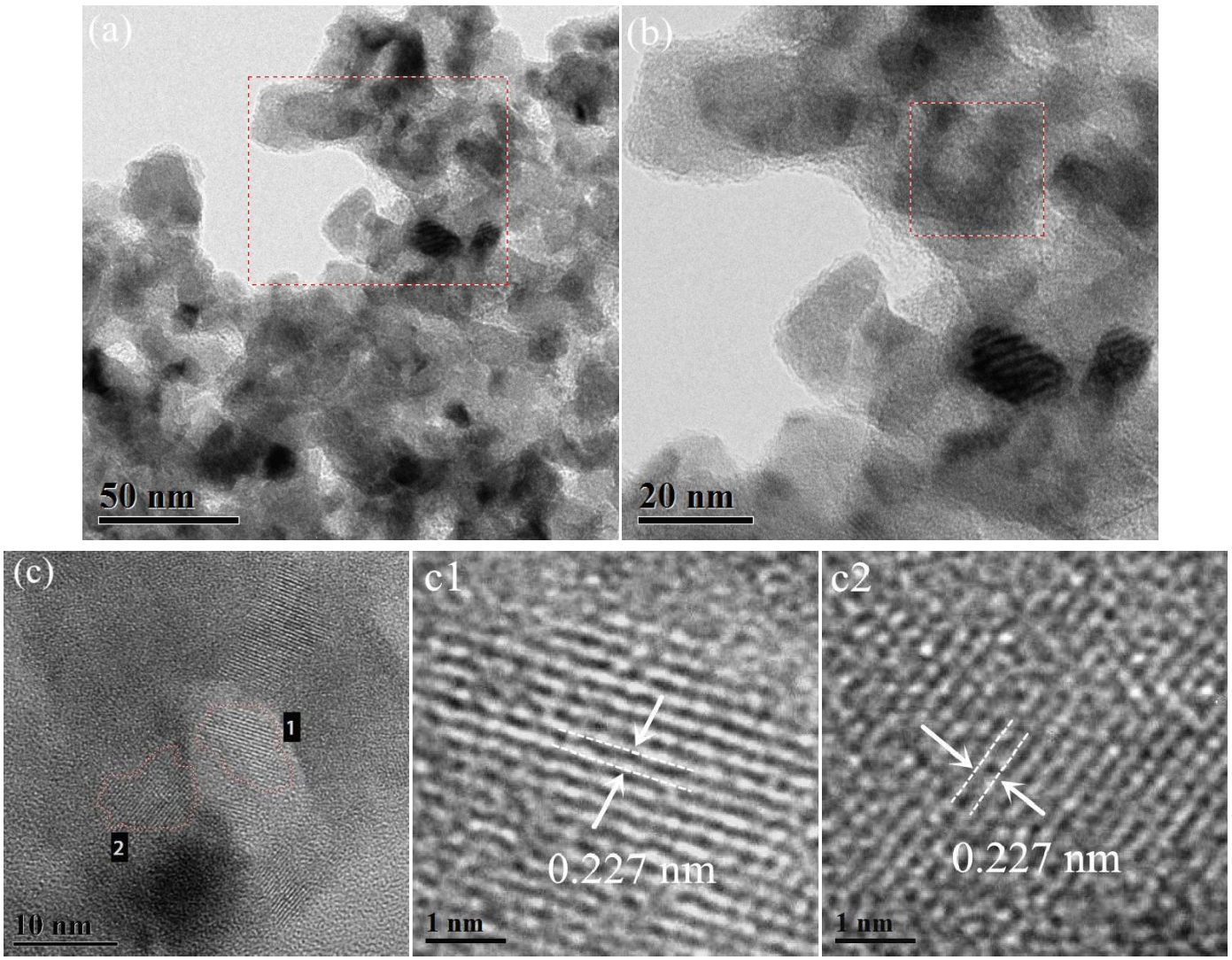

Figure 3. (a) TEM images of Pt@TiNiN catalyst, (b) enlarged TEM image marked in (a), (c) enlarged TEM marked in (b). (c1, c2) HR-TEM images with high magnification of the selected part marked in (c).

Figure 4 shows the diffraction patterns of the Pt@TiN and Pt@TiNiN catalysts, all the diffraction peaks could be attributed to the TiN (fcc) structure, no any Pt diffraction peaks could be observed on the patterns. However, the TEM-EDX profile (SI, Figure S4 and S5) revealed that the averaged weight percentage of Pt of the Pt@TiN and Pt@TiNiN nanoparticles was 5.09% and 4.98%, respectively. Furthermore, the overall Pt loadings for Pt@TiN and Pt@TiNiN catalysts are 5.15 wt% and 5.06 wt%, corresponding to the 5.53 μgcm^{-2} and 5.44 μgcm^{-2}, respectively, as determined by ICP-OES test, which agrees well with the EDX results. If the dispersing of Pt on the surface of the nitrides is considered as an uniform dispersion, the calculated

thickness of the Pt layers are 0.11 nm and 3/10 atoms thicknesses, respectively, based on surface area of the supported TiNiN NPs supported on the GC. Clearly, the deposited Pt exists on the surface of the nitrides as either extra-thin layer or amorphous layer/nanoparticles, but the clear lattice fringes deny the existence of amorphous Pt nanoparticles/layers. Thus, the most probably existence state of Pt on the nitrides nanoparticles is extra-thin layer, which can be further confirmed/supported by the ultra-high performance of the catalysts (discussed later).

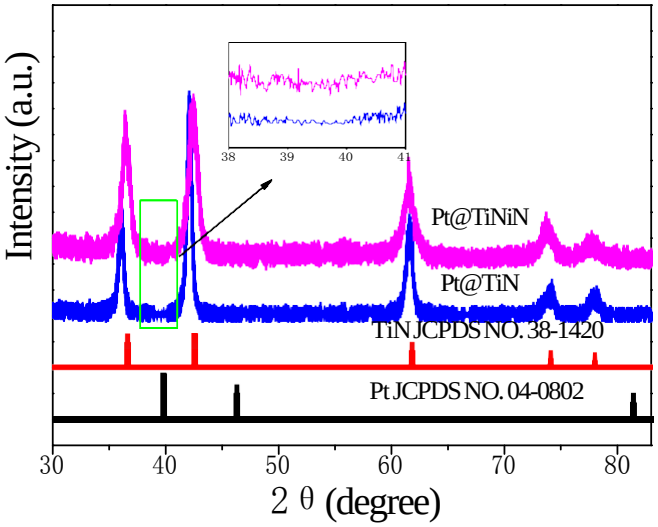

Figure 4. XRD patterns of Pt@TiN and Pt@TiNiN catalysts, and insert is the enlarged pattern of the part marked.

Figure 5 shows the XPS spectra of Pt@TiN and Pt@TiNiN catalysts. Each Pt 4f peak can be deconvoluted into two pairs of doublets, according to the deconvoluted results, large amount of Pt atoms exist as Pt (II) in the Pt@TiN catalyst, while existed mainly as Pt (0) in Pt@TiNiN through comparing the relative integrated areas Pt (0) and Pt (II) peaks, suggesting that Ni element doping can significantly increase the atom ration of Pt(0) in the catalyst, it may be one of the main reasons of the superior performance of Pt@TiNiN to Pt@TiN catalyst. In the Pt 4f XPS spectra of the Pt@TiNiN catalyst (Figure 4), the strong interaction between Pt and TiNiN was evidenced by the clear shift in the Pt $4f_{7/2}$ peak to a lower binding

energy (70.8 eV) as compared with that for the commercial Pt/C (71.2 eV) catalyst. The negative shift of the Pt 4f binding energy implied that the Pt NPs can get electrons from the TiNiN NPs [46, 47], which will lead to a down-shift in the d-band center of Pt, suggesting that the electronic structure of Pt atoms can be modified by Ni doping.

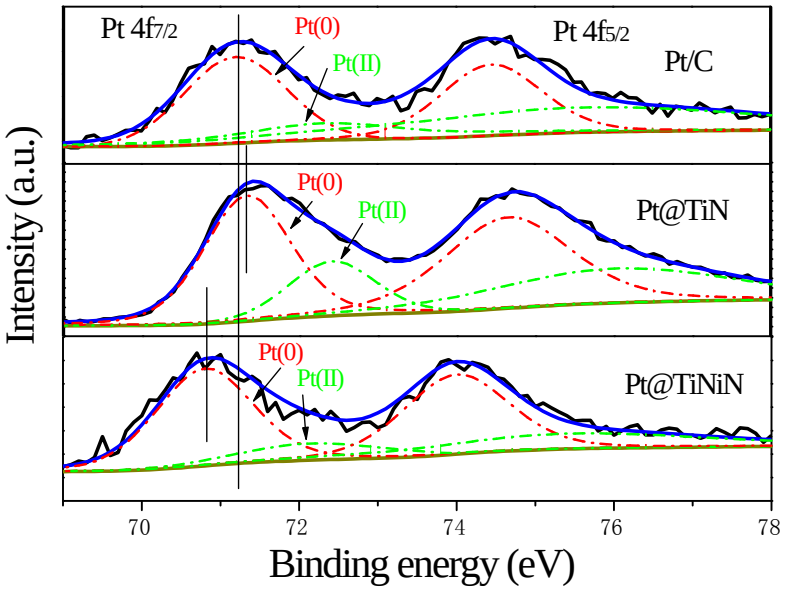

Figure 5. The Pt 4f XPS spectra of the Pt/C, Pt@TiN and Pt@TiNiN catalysts.

Figure 6a shows the CV curves of Pt/C, Pt@TiN and Pt@TiNiN catalysts in nitrogen saturated 0.5 M H_2SO_4 solution, the electrochemically active area (ECSA) of the catalysts could be obtained by calculating the charge through the hydrogen underpotential depsorption (H_{UPD}) area [48]. The calculated ECSAs of Pt@TiN and Pt@TiNiN are 94 and 97 m^2 g Pt^{-1}, respectively, which are both about 1.7 times of that of the Pt/C catalyst (55.4 m^2 g Pt^{-1}). The larger ECSA of Pt for the Pt@TiN and Pt@TiNiN catalysts was most likely due to the high dispersion of the Pt that creates a large Pt surface, further confirming that the Pt may be existed on the surface of nitrides as extra-thin layer.

Figure 6b shows the polarization curves of Pt/C, Pt@TiN and Pt@TiNiN catalyst in a 0.1 M $HClO_4$ solution saturated with oxygen, using a rotating disk electrode (RDE) at 1600 rpm, and the current density was normalized to the geometric surface area of the electrodes. As shown in Figure 6b, Pt@TiN and

Pt@TiNiN both show better catalytic activity toward the ORR than that of the JM Pt/C catalyst with the same Pt loadings. The half wave potential measured from the ORR polarization curves for Pt@TiNiN catalyst was 893 mV, which was 16 mV and 44 mV higher than that of Pt@TiN and Pt/C catalyst, respectively. Furthermore, the onset potential of Pt@TiNiN is 20 mV positive-shifted compared with the Pt/C catalyst even within the same catalyst loadings (Figure 6c).

For a better understanding of the observed catalytic activities of the synthesized electrocatalysts for the ORR, the mass activities and specific activity at 0.90 V were calculated on the basis of the ORR polarization curves. The kinetic current was calculated from the ORR polarization curves by using the Koutecky−Levich equation [49]: $1/i = 1/i_k + 1/i_d$ (where i_k is the kinetic current and i_d is the diffusion-limiting current). The mass activity was obtained by normalizing the kinetic current to the Pt loading, and the specific activity was got by normalizing the kinetic current to the ECSA. The mass activity comparison of Pt/C, Pt@TiN and Pt@TiNiN are shown in Figure 6d, where one can see that Pt@TiNiN exhibits a mass activity of 0.83 Amg^{-1}_{Pt}, which is 4 times greater than that of Pt/C catalyst. At the same time, the specific activity of Pt@TiNiN was 0.57 $mAcm^{-2}$, which is also much higher than Pt/C and Pt@TiN catalysts.

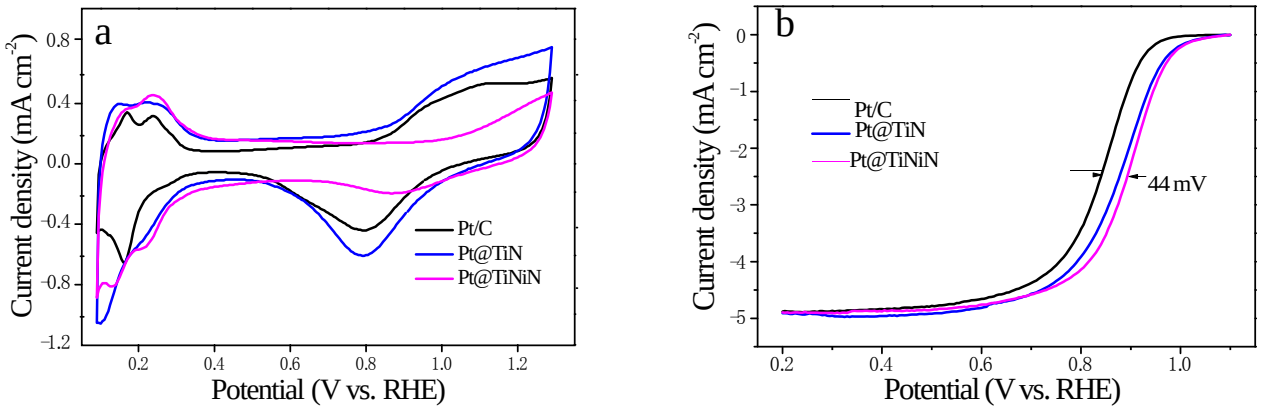

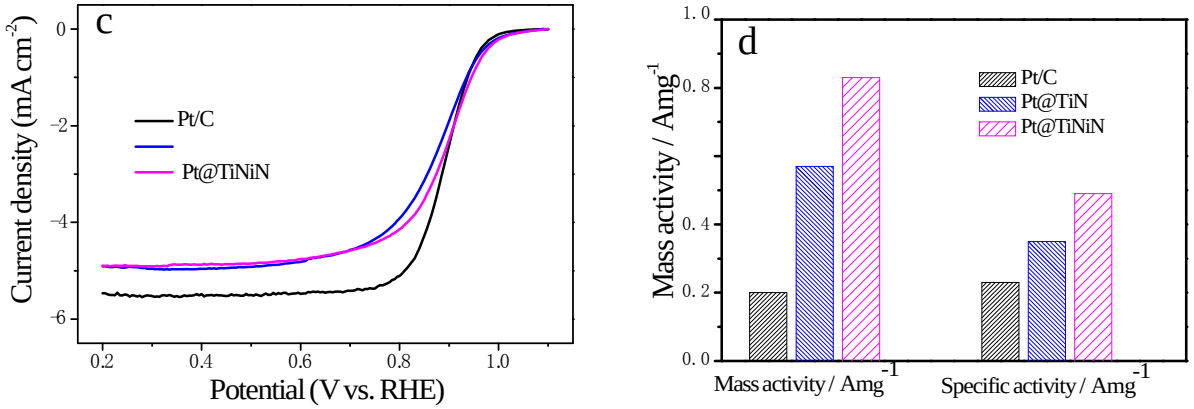

Figure 6. (a) CVs of Pt/C, Pt@TiN and Pt@TiNiN catalysts, recorded at room temperature in N_2-purged 0.5 M H_2SO_4 solution at a scan rate of 50 mVs^{-1}, and the Pt loading for Pt/C, Pt@TiN and Pt@TiNiN were 5.61, 5.53 and 5.44 μgcm^{-2}, respectively, (b) The polarization curves of Pt/C, Pt@TiN and Pt@TiNiN catalysts in 0.1 M $HClO_4$ solution saturated with O_2, using a RDE at 1600 rpm at a scan rate of 10 mVs^{-1}, (c) The polarization curves of Pt/C, Pt@TiN and Pt@TiNiN catalysts with the same catalyst loading: 0.10 $mgcm^{-2}$ for all the samples, and (d) mass and specific activities for Pt/C, Pt@TiN and Pt@TiNiN catalysts.

Waiting for the results of XANS and STEM.

Compared with the Pt@TiN catalyst, the Pt@TiNiN catalyst exhibited a significant improved ORR activity, indicating Ni element doping had a positive effect towards the ORR activity. As shown in Figure 6a, , Pt@TiNiN catalyst exhibited much lower Pt oxidation current at high potential region than JM Pt/C and Pt@TiN catalysts. The positive shifted Pt oxidation potential demonstrated the weakened interaction between Pt itself and the intermediate oxide species, caused by the down-shift in the d-band center of Pt [48, 50]. Furthermore, it worth noting that, from previous studies [37, 51], OH groups can be adsorbed on the TiN surface, e.g., TiN or TiNiN support could lower the amount of potentially OH coverage on supported Pt by inducing lateral repulsion between OH species on Pt atoms and neighboring OH species adsorbed on TiN/TiNiN NPs. In principle, decreasing OH coverage on Pt will reduce the overpotential for ORR and the weakened interaction between Pt itself and the intermediate oxide species will introduce a balance between O-O bond breaking and the removal of surface oxides [52, 53], resulting in the superior ORR performance

of Pt@TiNiN to the Pt@TiN.

The stability/durability of the catalysts was evaluated by potential cycling between 0.6 and 1.05 V for 10,000 cycles in an O_2-saturated 0.5 M H_2SO_4 solution at a scan rate of 50 mV s^{-1}. The evolutions of CV curves for Pt/C and Pt@TiNiN obtained after every 2, 000 cycles are shown in Figure 7a and b, respectively. It was observed that the ECSA of Pt/C dropped almost 26% after the first 2, 000 cycles, and then the decay rate slowed down with continued cycling, and the final ECSA after 10, 000 cycles dropped about 55% of the initial value. However, the Pt@TiNiN sample shows great improvement on ECSA preservation, with 78% of the initial ECSA remaining after 10, 000 cycles (Figure 7c).

Furthermore, we also investigated the stability/durability of the catalysts by ORR cycling testing, after 10,000 ORR potential cycles, the Pt/C catalyst showed a degradation of more than 25 mV in its half-wave potential, $E_{1/2}$ (Figure 7d), while the degradation of the Pt@TiNiN catalyst was much lower, with less than a 10 mV negative shift in the half-wave potential, indicating that Pt@TiNiN is much more durable and stable than the Pt/C catalyst.

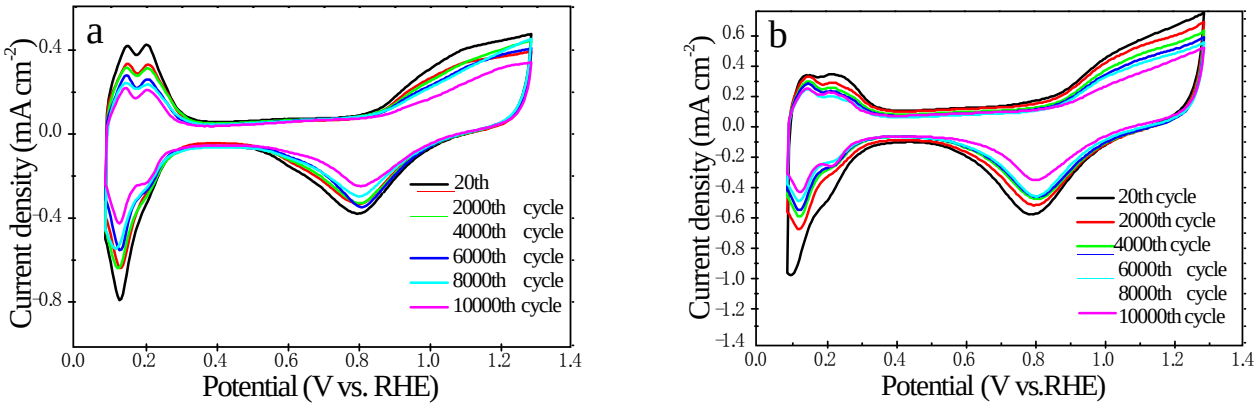

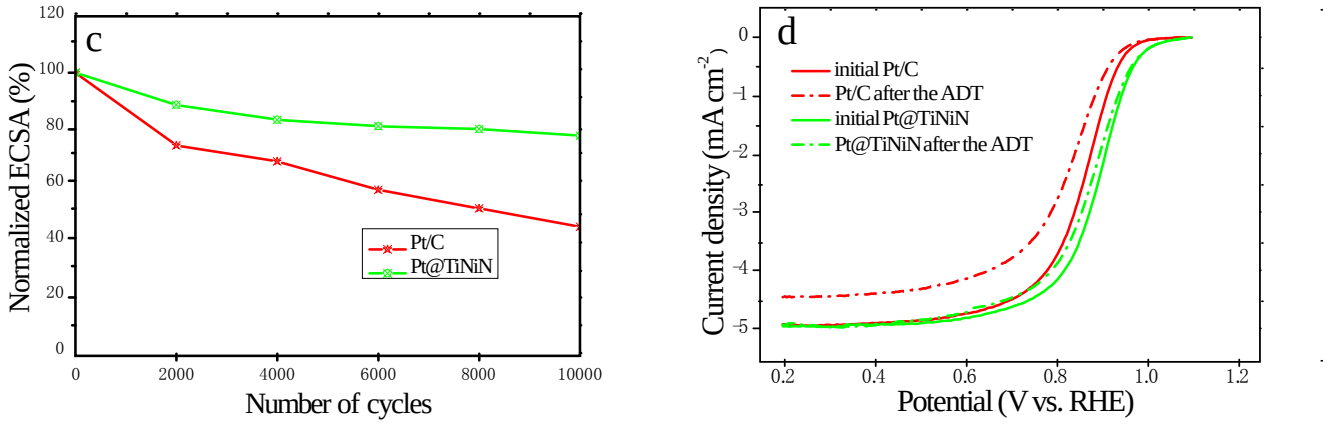

Figure 6. (a) and (b) show the evolutions of CV curves after various cycles for Pt/C and Pt@TiNiN, respectively, (c) Comparison of ECSA loss for Pt/C and Pt@TiNiN and (d) Polarization curves of Pt/C and Pt@TiNiN before (solid curves) and after (dashed curves) the ADT test.

The excellent stability of Pt@TiNiN catalyst after 10,000 electrochemical cycles was also verified by TEM images. As shown in Figure S6(a-c), compared with the TEM images of Pt@TiNiN before potential cycling (Figure 3), although some coalesced and/or aggregated Pt nanoparticles were observed, the Pt layer and TiNiN structure were preserved (Figure S6(d-e). Furthermore, the EDS profile of Pt@TiNiN revealed that only a slight Pt loss after the ADT (SI, Figure S7). As to Pt/C catalyst, however, the averaged Pt size increases from 3.2 nm to 8.7 nm (SI, Figure S8), and a significant decrease of Pt density on carbon support were observed after the ADT, implying that the major cause for ECSA loss and ORR loss of Pt/C was Pt detaching and ripening issues related to carbon-support corrosion [31, 54]. Although the exact essence of Pt stability for Pt@TiNiN catalyst is still not well understood, it is plausible to hypothesize the strong Pt–TiNiN interaction alters the electronic structure of the Pt atoms, which causes the shift of the Pt $4f_{7/2}$ peak to lower binding energies, thereby creating a stabilizing effect against Pt oxidation/dissolution. Thus, the oxidation of Pt atoms on TiNiN becomes more difficult than that on carbon support, which can be confirmed by the comparison of the CV curves of the three catalysts, where a higher Pt oxidation potential can be observed for Pt@TiNiN catalyst (Figure 6a). Another reason is the better stability of nitrides against oxidation/corrosion than carbon materials [42, 44].

4. Conclusions

In conclusion, we have developed a robust carbon-free Pt@TiNiN catalyst by a two stage approach: prepared nitride nanoparticles with small particle size by nitriding the ammonia complex of transition metal, followed by depositing an extra-thin Pt layer on the nitride nanoparticles with a pulse deposition method. the catalyst exhibited outstanding ORR activity and stability. Compared with commercial Pt/C catalyst, with carbon as support and Pt being nanoparticles, our catalyst exhibits much higher Pt dispersion and utilization, as well as much high stability due to no carbon corrosion problems. what's more, our catalyst is not only much cheaper, but also eliminates issues related to carbon-support corrosion even respected to the carbon supported core-shell catalyst with precious metal NPs as core. It is found that the addition of nickel could improve the ORR performance of the catalyst significantly. We suggest that the great performance improvement is probably due to the high dispersion and utilization of Pt, the synergistic effect introduced by the Ni doping, the excellent stability of nitrides, and the strong interaction between Pt layer and the TiNiN support. The approach and the catalyst may provide a novel pathway to develop low-cost, carbon-free, high stability and low platinum electrocatalyst for fuel cell application.

References

[1] Y. Liu, W.E. Mustain, Journal of the American Chemical Society 135 (2013) 530-533.

[2] D.H. Youn, G. Bae, S. Han, J.Y. Kim, J.-W. Jang, H. Park, S.H. Choi, J.S. Lee, Journal of Materials Chemistry A 1 (2013) 8007.

[3] H. Peng, Z. Mo, S. Liao, H. Liang, L. Yang, F. Luo, H. Song, Y. Zhong, B. Zhang, Scientific reports 3 (2013).

[4] H. Peng, S. Hou, D. Dang, B. Zhang, F. Liu, R. Zheng, F. Luo, H. Song, P. Huang, S. Liao, Applied Catalysis B: Environmental 158-159 (2014) 60-69.

[5] J. Greeley, I.E.L. Stephens, A.S. Bondarenko, T.P. Johansson, H.A. Hansen, T.F. Jaramillo, J. Rossmeisl, I. Chorkendorff, J.K. Norskov, Nature Chemistry 1 (2009) 552-556.

[6] V.R. Stamenkovic, B. Fowler, B.S. Mun, G. Wang, P.N. Ross, C.A. Lucas, N.M. Markovic, Science 315

(2007) 493-497.

[7] S.J. Liao, K.A. Holmes, H. Tsaprailis, V.I. Birss, Journal of the American Chemical Society 128 (2006) 3504-3505.

[8] Y. Liang, H. Wang, P. Diao, W. Chang, G. Hong, Y. Li, M. Gong, L. Xie, J. Zhou, J. Wang, T.Z. Regier, F. Wei, H. Dai, Journal of the American Chemical Society 134 (2012) 15849-15857.

[9] V.R. Stamenkovic, B.S. Mun, K.J.J. Mayrhofer, P.N. Ross, N.M. Markovic, Journal of the American Chemical Society 128 (2006) 8813-8819.

[10]D. Wang, H.L. Xin, R. Hovden, H. Wang, Y. Yu, D.A. Muller, F.J. DiSalvo, H.D. Abruna, Nature materials 12 (2013) 81-87.

[11]P. Strasser, S. Koh, T. Anniyev, J. Greeley, K. More, C. Yu, Z. Liu, S. Kaya, D. Nordlund, H. Ogasawara, M.F. Toney, A. Nilsson, Nature Chemistry 2 (2010) 454-460.

[12]T. Ghosh, M.B. Vukmirovic, F.J. DiSalvo, R.R. Adzic, Journal of the American Chemical Society 132 (2010) 906-+.

[13]R.R. Adzic, J. Zhang, K. Sasaki, M.B. Vukmirovic, M. Shao, J.X. Wang, A.U. Nilekar, M. Mavrikakis, J.A. Valerio, F. Uribe, Topics in Catalysis 46 (2007) 249-262.

[14]K. Sasaki, K.A. Kuttiyiel, D. Su, R.R. Adzic, Electrocatalysis 2 (2011) 134-140.

[15]J.X. Wang, H. Inada, L.J. Wu, Y.M. Zhu, Y.M. Choi, P. Liu, W.P. Zhou, R.R. Adzic, Journal of the American Chemical Society 131 (2009) 17298-17302.

[16]C. Xu, R. Wang, M. Chen, Y. Zhang, Y. Ding, Physical chemistry chemical physics : PCCP 12 (2010) 239-246.

[17]D. Wang, Y. Yu, H.L. Xin, R. Hovden, P. Ercius, J.A. Mundy, H. Chen, J.H. Richard, D.A. Muller, F.J. DiSalvo, H.D. Abruna, Nano letters 12 (2012) 5230-5238.

[18]S. Guo, S. Zhang, D. Su, S. Sun, Journal of the American Chemical Society 135 (2013) 13879-13884.

[19]X. Zhao, S. Chen, Z. Fang, J. Ding, W. Sang, Y. Wang, J. Zhao, Z. Peng, J. Zeng, Journal of the

American Chemical Society 137 (2015) 2804-2807.

[20]K. Sasaki, H. Naohara, Y. Choi, Y. Cai, W.F. Chen, P. Liu, R.R. Adzic, Nature communications 3 (2012) 1115.

[21]D. Dang, H. Zou, Z.a. Xiong, S. Hou, T. Shu, H. Nan, X. Zeng, J. Zeng, S. Liao, ACS Catalysis 5 (2015) 4318-4324.

[22]X. Lu, F. Luo, H. Song, S. Liao, H. Li, Journal of Power Sources 246 (2014) 659-666.

[23]K.A. Kuttiyiel, K. Sasaki, Y. Choi, D. Su, P. Liu, R.R. Adzic, Energy & Environmental Science 5 (2012) 5297.

[24]D. Dang, S. Liao, F. Luo, S. Hou, H. Song, P. Huang, Journal of Power Sources 260 (2014) 27-33.

[25]D. Chen, R. Chen, D. Dang, T. Shu, H. Peng, S. Liao, Electrochemistry Communications 46 (2014) 115-119.

[26]M. Huang, G. Dong, N. Wang, J. Xu, L. Guan, Energy & Environmental Science 4 (2011) 4513.

[27]L. Yang, M.B. Vukmirovic, D. Su, K. Sasaki, J.A. Herron, M. Mavrikakis, S. Liao, R.R. Adzic, The Journal of Physical Chemistry C 117 (2013) 1748-1753.

[28]B.Y. Xia, N. Wan Theng, H.B. Wu, X. Wang, X.W. Lou, Angewandte Chemie-International Edition 51 (2012) 7213-7216.

[29]S. Chen, Z. Wei, X. Qi, L. Dong, Y.G. Guo, L. Wan, Z. Shao, L. Li, Journal of the American Chemical Society 134 (2012) 13252-13255.

[30]M. Yang, A.R. Van Wassen, R. Guarecuco, H.D. Abruña, F.J. DiSalvo, Chemical communications 49 (2013) 10853.

[31]D.P. He, S.C. Mu, M. Pan, Carbon 49 (2011) 82-88.

[32]H. Van Thi Thanh, K.C. Pillai, H.-L. Chou, C.-J. Pan, J. Rick, W.-N. Su, B.-J. Hwang, J.-F. Lee, H.-S. Sheu, W.-T. Chuang, Energy & Environmental Science 4 (2011) 4194-4200.

[33]A.-L. Wang, H. Xu, J.-X. Feng, L.-X. Ding, Y.-X. Tong, G.-R. Li, Journal of the American Chemical

Society 135 (2013) 10703-10709.

[34]R. Kumar, S. Pasupathi, B.G. Pollet, K. Scott, Electrochimica Acta 109 (2013) 365-369.

[35]J. Chen, K. Takanabe, R. Ohnishi, D. Lu, S. Okada, H. Hatasawa, H. Morioka, M. Antonietti, J. Kubota, K. Domen, Chemical communications 46 (2010) 7492-7494.

[36]B. Avasarala, T. Murray, W. Li, P. Haldar, Journal of Materials Chemistry 19 (2009) 1803.

[37]M.M.O. Thotiyl, S. Sampath, Electrochimica Acta 56 (2011) 3549-3554.

[38]M. Yang, Z. Cui, F.J. DiSalvo, Physical chemistry chemical physics : PCCP 15 (2013) 7041-7044.

[39]Z. Cui, M. Yang, F.J. DiSalvo, Acs Nano 8 (2014) 6106-6113.

[40]Z. Cui, R.G. Burns, F.J. DiSalvo, Chemistry of Materials 25 (2013) 3782-3784.

[41]M. Yang, R. Guarecuco, F.J. DiSalvo, Chemistry of Materials 25 (2013) 1783-1787.

[42]M. Yang, Z. Cui, F.J. DiSalvo, Physical Chemistry Chemical Physics 15 (2013) 1088-1092.

[43]M.H. Yang, F.J. DiSalvo, Chemistry of Materials 24 (2012) 4406-4409.

[44]Y. Dong, Y. Wu, M. Liu, J. Li, ChemSusChem 6 (2013) 2016-2021.

[45]Y. Li, Y. Li, E. Zhu, T. McLouth, C.Y. Chiu, X. Huang, Y. Huang, Journal of the American Chemical Society 134 (2012) 12326-12329.

[46]V.T. Ho, C.J. Pan, J. Rick, W.N. Su, B.J. Hwang, Journal of the American Chemical Society 133 (2011) 11716-11724.

[47]C. Wang, H. Daimon, S.H. Sun, Nano letters 9 (2009) 1493-1496.

[48]K.A. Kuttiyiel, K. Sasaki, Y. Choi, D. Su, P. Liu, R.R. Adzic, Nano letters 12 (2012) 6266-6271.

[49]S.P. Hsu, C.W. Liu, H.S. Chen, T.Y. Chen, C.M. Lai, C.H. Lee, J.F. Lee, T.S. Chan, L.D. Tsai, K.W. Wang, Electrochimica Acta 105 (2013) 180-187.

[50]H. Liu, C. Koenigsmann, R.R. Adzic, S.S. Wong, Acs Catalysis 4 (2014) 2544-2555.

[51]M.M. Ottakam Thotiyl, T. Ravikumar, S. Sampath, Journal of Materials Chemistry 20 (2010) 10643.

[52]V. Stamenkovic, B.S. Mun, K.J.J. Mayrhofer, P.N. Ross, N.M. Markovic, J. Rossmeisl, J. Greeley, J.K.

Nørskov, Angewandte Chemie 118 (2006) 2963-2967.

[53]F.H.B. Lima, J. Zhang, M.H. Shao, K. Sasaki, M.B. Vukmirovic, E.A. Ticianelli, R.R. Adzic, Journal of Physical Chemistry C 111 (2007) 404-410.

[54] S.-Y. Huang, P. Ganesan, B.N. Popov, ACS Catalysis 2 (2012) 825-831.